

Faculty Scholarship

---

6-1-1995

## Purification of a Variant-specific Surface Protein of *Giardia lamblia* and Characterization of its Metal-binding Properties

Mark R. Chance

*Case Western Reserve University*, [mark.chance@case.edu](mailto:mark.chance@case.edu)

Author(s) ORCID Identifier:


[Mark R. Chance](#)

Follow this and additional works at: <https://commons.case.edu/facultyworks>

Digital Part of the [Medicine and Health Sciences Commons](#)  
Commons

---

### Network Recommended Citation

 Hugo D. Luján, Michael R. Mowatt, Jing-jing Wu, Yun Lu, Andrew Lees, Mark R. Chance, Theodore E. Nash. Purification of a Variant-specific Surface Protein of *Giardia lamblia* and Characterization of its Metal-binding Properties. *Journal of Biological Chemistry*, Volume 270, Issue 23, 1995, Pages 13807-13813, <https://doi.org/10.1074/jbc.270.23.13807>.

This Article is brought to you for free and open access by Scholarly Commons @ Case Western Reserve University. It has been accepted for inclusion in Faculty Scholarship by an authorized administrator of Scholarly Commons @ Case Western Reserve University. For more information, please contact [digitalcommons@case.edu](mailto:digitalcommons@case.edu).

CWRU authors have made this work freely available. [Please tell us](#) how this access has benefited or impacted you!

# Purification of a Variant-specific Surface Protein of *Giardia lamblia* and Characterization of its Metal-binding Properties\*

(Received for publication, October 11, 1994, and in revised form, April 5, 1995)

Hugo D. Luján<sup>‡§</sup>, Michael R. Mowatt<sup>‡</sup>, Jing-jing Wu<sup>¶</sup>, Yun Lu<sup>¶</sup>, Andrew Lees<sup>||</sup>, Mark R. Chance<sup>¶</sup>, and Theodore E. Nash<sup>‡</sup>

From the <sup>‡</sup>Laboratory of Parasitic Diseases, NIAID, National Institutes of Health, Bethesda, Maryland 20892-0425, the <sup>¶</sup>Albert Einstein College of Medicine of Yeshiva University, Bronx, New York 10461, and the <sup>||</sup>Department of Medicine, Uniformed Services University of the Health Sciences, Bethesda, Maryland 20814

***Giardia lamblia*, an intestinal parasite of humans and other vertebrates, undergoes surface antigenic variation by modulating the expression of different variant-specific surface proteins (VSP). VSPs are cysteine-rich surface proteins that bind zinc and other heavy metals *in vitro*. We developed an immunoaffinity chromatographic method to purify a VSP in order to determine its biochemical properties. The sequences of two different proteolytic fragments agreed with the sequence deduced from the cloned gene, and amino-terminal sequence indicated the removal of a 14-residue signal peptide, consistent with the transport of VSP to the cell surface. The protein is not glycosylated and has an isoelectric point of 5.3. X-ray microanalyses indicated that the major metals in *Giardia* trophozoites, as well as purified VSP, are zinc and iron. The zinc concentration in *Giardia* cells was found to be 0.43 mM and the iron concentration 0.80 mM when compared with standard samples (zinc) or calculated from a known physical constants (iron). We propose that metal coordination stabilizes VSPs, rendering them resistant to proteolytic attack in the upper small intestine. Moreover, the ability to bind ions by *Giardia* may play a role in nutritional deficiency and/or malabsorption in heavily infected persons.**

*Giardia lamblia* is a binucleate flagellated protozoan that causes acute and chronic intestinal infections in humans and other vertebrates (1). Infections due to *Giardia* are among the most common human infections worldwide, and in developing countries most children are continually infected or reinfected. Clinical manifestations vary from asymptomatic infection to severe diarrhea and malabsorption (1, 2).

The entire surface of a *Giardia* trophozoite, including the adhesive disk and flagella, is covered by a protein coat (3, 4) composed of a single variant-specific surface protein (VSP)<sup>1</sup> (5). During trophozoite growth this VSP may be replaced with another antigenically distinct VSP (6). This surface antigenic variation occurs spontaneously *in vitro* (7), *i.e.* in the absence of known selective pressure, and has been demonstrated in ex-

perimental infections of humans (8) and laboratory animals (9). The potential antigenic variability is encoded in the VSP gene repertoire, the minimum size of which has been estimated as 133 (10). The mechanism by which *Giardia* modulates the expression of different VSP genes, and thereby effects antigenic variation, is unknown.

With some notable exceptions (11–14), biochemical properties of VSPs have been deduced from amino acid sequences predicted from cloned cDNAs or genes. Analysis of these sequences showed that VSPs are rich in cysteine (typically 12 mol %; Fig. 1), which is found primarily in Cys-X-X-Cys tetrapeptides distributed nonrandomly throughout the polypeptide (13). Sequence comparisons indicated that, in contrast to the variability observed among amino-terminal regions, carboxyl-terminal primary structure, including the putative transmembrane domain, is highly conserved among VSPs (Ref. 15 and Fig. 1). Although all VSPs contain at least one consensus N-linked glycosylation site, the glycosylation status of these molecules is unknown. In addition, Nash (5) identified zinc-binding motifs in VSPs and suggested that the sequestration of zinc by VSPs could contribute to some of the symptoms of clinical giardiasis and zinc malnutrition. Recently, the ability of these proteins to bind <sup>65</sup>Zn *in vitro* was reported by two independent groups (13, 14). Like other metal-binding proteins, VSPs can bind different cations, including Cd<sup>2+</sup>, Co<sup>2+</sup>, Cu<sup>2+</sup>, Fe<sup>2+</sup>, and Mn<sup>2+</sup> (13, 14). Unlike other similar metal-binding proteins, VSPs are localized on the cell surface.

The function of VSPs is unknown, but the features conserved among VSPs suggest that these proteins play an important role in *Giardia* biology. Direct biochemical analyses of purified, native VSP would greatly enhance our understanding of VSP structure and function.

Here we report a simple method for the purification of a VSP from the *Giardia* isolate GS/M, clone H7, by immunoaffinity chromatography. Our results verify the expression of the protein predicted from the cloned VSP H7 cDNA and indicate that VSP H7 is processed by cleavage of a 14-residue amino-terminal signal peptide. The purified protein contains the COOH-terminal pentapeptide conserved among all VSPs and, furthermore, is not glycosylated. Consistent with our previous metal-binding studies, we confirm that native VSP binds zinc and iron, most likely by coordination to cysteinyl sulfurs.

## EXPERIMENTAL PROCEDURES

**Parasites**—The origin of the *G. lamblia* GS/M isolate and derivation of the H7 clone has been reported (16). Trophozoites were cultured axenically at 37 °C in Diamond's medium TYI-S-33 supplemented with 10% adult bovine serum and 0.5 mg of bovine bile/ml (17). Cultures were grown to confluence in 8-ml glass tubes. The medium and nonadherent trophozoites were discarded and replaced with the same volume of ice-cold phosphate-buffered saline containing 1 mM of L-cysteine and 20 μg/ml of bathocuproine sulfonate (PBS-Cys) (18). The tubes were chilled for 15

\* The costs of publication of this article were defrayed in part by the payment of page charges. This article must therefore be hereby marked "advertisement" in accordance with 18 U.S.C. Section 1734 solely to indicate this fact.

§ To whom correspondence should be addressed: Laboratory of Parasitic Diseases, NIAID, NIH, 9000 Rockville Pike, Bldg. 4, Rm. 126, Bethesda, MD 20892-0425. Tel.: 301-496-6920. Fax: 301-402-2689.

<sup>1</sup> The abbreviations used are: VSP, variant-specific surface protein; PBS, phosphate-buffered saline; mAb, monoclonal antibody; EXAFS, extended x-ray absorption fine structure; ZnTPP, zinc-mesotetraphenylporphyrin; ZnS, zinc sulfide; HPLC, high performance liquid chromatography; TLCK, 1-chloro-3-tosylamido-7-amino-2-heptanone; PAGE, polyacrylamide gel electrophoresis.

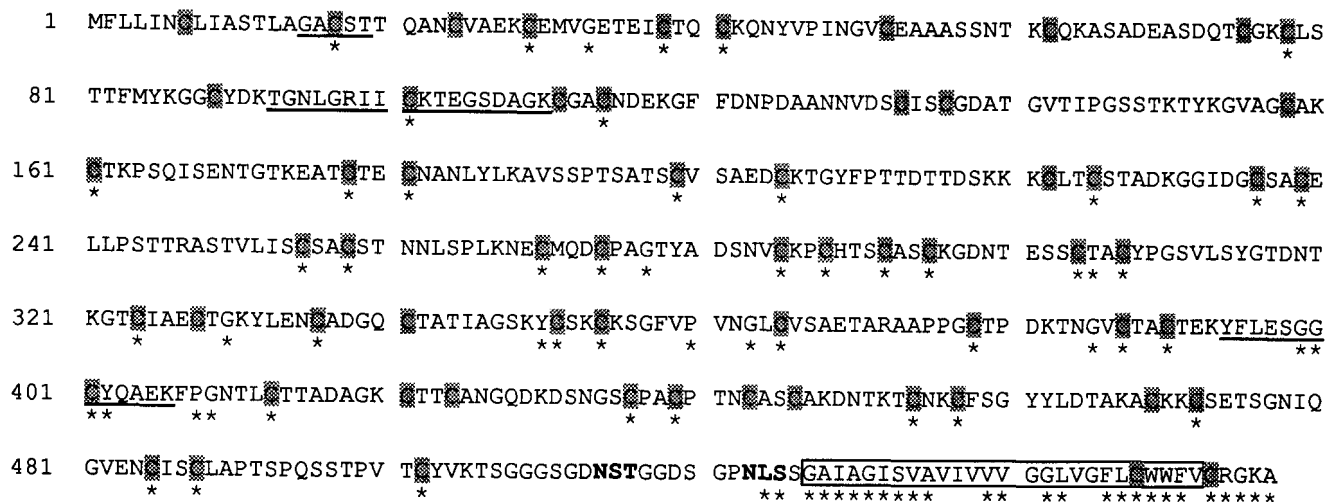


Fig. 1. Amino acid sequence of VSP H7 deduced from a cloned cDNA and peptides sequenced from purified VSP H7. The amino acid sequence of VSP H7 as deduced from a cloned cDNA (GenBank<sup>®</sup> accession number M80480) is shown with cysteine residues shaded. Underlining indicates peptide sequences determined from purified VSP H7. Bold type designates consensus N-linked glycosylation sites. A box surrounds the putative transmembrane domain, and asterisks designate residues conserved among the six deduced VSP sequences (VSP A6, VSP 1267, VSP H7, CRP 72, TSP 11, and TSA 417; GenBank accession numbers M63966, M80480, M83933, M95814, and M33641, respectively) as determined by the GCG program PILEUP.

min, inverted 10 times, and the trophozoites counted with a Coulter model ZB1 electronic counter (Coulter Electronic, Hialeah, FL). Surface antigenic homogeneity of the harvested cells was deemed greater than 95% by indirect immunofluorescence using mAb G10/4 (16).

**VSP Purification**—All steps in the purification procedure were performed at 4 °C. Trophozoites ( $5\text{--}6 \times 10^{10}$  cells) were washed twice with ice-cold PBS-Cys and lysed in 1 ml of buffer A (0.10 M sodium carbonate, pH 7.2, 0.05% *n*-butyl alcohol, 0.1% Thesit, 5  $\mu\text{g}/\text{ml}$  leupeptin, 100  $\mu\text{M}$  TLCK, 100  $\mu\text{M}$  phenylmethylsulfonyl fluoride) by incubation at 4 °C for 2 h. Cell ghosts were sedimented at  $14,000 \times g$  for 60 min at 4 °C, and the supernatant stored at  $-70$  °C until used (within 1 week).

The mAb G10/4 (IgG<sub>1</sub>) (16) was purified from ascites by chromatography on protein G Plus-agarose (Pierce). The IgG fraction (50 mg of protein at 10 mg/ml in 0.2 M carbonate buffer, pH 8.0) was immobilized on 5 ml of glutaraldehyde-activated Trisacryl<sup>®</sup> beads (IBF) according to the manufacturer's instructions. The column was then washed with 100 ml of PBS and stored in same buffer containing 0.02% sodium azide at 4 °C up to 3 months without loss of activity.

To purify the VSP, 1 ml of *Giardia*-soluble proteins in buffer A (about 100 mg) was loaded at a flow rate of 0.5 ml/h onto the affinity column (5-ml column volume, 10-mm diameter) pre-equilibrated with 100 ml of buffer A. The column was washed under the same conditions with 200 ml of buffer A, and bound VSP was eluted with buffer B (0.10 M glycine, pH 3.0, 0.05% *n*-butyl alcohol, 0.1% Thesit, 5  $\mu\text{g}/\text{ml}$  leupeptin, 100  $\mu\text{M}$  TLCK, 100  $\mu\text{M}$  phenylmethylsulfonyl fluoride). Proteins in the fractionated eluate were detected spectrophotometrically at 280 nm, and fractions containing the VSP were pooled. Pooled samples were concentrated, the buffer exchanged for PBS-0.01% Thesit using Centricon 10 concentrators (Amicon), and stored at  $-70$  °C.

For subsequent analyses, VSP was precipitated by addition of ice-cold acetone to a final concentration of 50% (v/v), washed once with acetone at  $-20$  °C, and air-dried. Precipitated samples were resuspended in 0.1% SDS at a final concentration of approximately 1 mg/ml, determined by Bio-Rad DC protein assay calibrated with bovine serum albumin as a standard.

**Amino Acid Sequence Analysis**—Amino-terminal sequences were determined from purified VSP H7 spotted onto PVDF membrane (Applied Biosystems, Inc.) by Edman degradation on an automated Applied Biosystems 477A protein sequencer equipped with an on-line phenylthiohydantoin analyzer. Internal sequences from VSP H7 were determined by digestion of the purified protein with endoproteinase Lys-C and separation of peptides by narrowbore reversed phase chromatography on a Hewlett-Packard 1090 HPLC/1040A diode array detector using a Vydac C-18 column (2.1  $\times$  150 mm). Peptides were eluted with a gradient of 0.057% trifluoroacetic acid/acetonitrile, at a flow rate of 150  $\mu\text{l}/\text{min}$ . Gradient conditions were 5% B at 0 min to 33% B at 63 min, 60% B at 95 min and finally 80% B at 105 min. Peaks defined by an absorbance at 210 nm were collected and stored at  $-20$  °C before peptide sequence analysis. Amino-terminal sequences were determined as described above.

**Carbohydrate Analyses**—Carbohydrate analyses were performed on purified VSP and control buffer B (treated as the sample). Purified VSP (10  $\mu\text{g}/200$   $\mu\text{l}$ ) was dried under a stream of  $\text{N}_2$ , 100  $\mu\text{l}$  of 4 M trifluoroacetic acid added to the white residue, and heated at 100 °C for 4 h. Then, 10  $\mu\text{g}$  of VSP hydrolysate was injected into a pellicular anion exchange column (PA-1, 4  $\times$  250 mm) as described (19).

**Nucleotide and Amino Acid Sequence Analysis**—DNA Strider<sup>®</sup> 1.2 (20), AnalyzeSignalase 2.0.3 (21), BLASTP (22), and programs in the Genetics Computer Group package (23) running on the NIH Convex System were used to analyze the data.

**Peptide Synthesis and Conjugation**—VSP carboxyl-terminal peptides made on an Applied Biosystems, Inc. model 430 peptide synthesizer using Fmoc (*N*-(9-fluorenyl)methoxycarbonyl) chemistry were provided by the Biological Resources Branch, NIAID. Peptides were purified by reversed phase HPLC on Vydac C-18 columns and their identities verified by sequence and compositional analyses. Peptides A (H-FL-CRGKA-OH) and B (H-CFLC-acetoimidomethyl-RGKA-OH) were conjugated individually to both keyhole limpet hemocyanin (Sigma) and bovine serum albumin (Pentex) using *N*-iodoacetyl- $\beta$ -alanine-*N*-hydroxysuccinimide<sup>2</sup> and  $\gamma$ -maleimidobutyric acid *N*-hydroxysuccinimide ester (24), respectively. After dialysis against PBS, keyhole limpet hemocyanin conjugates were sterilized by passage through Millex-HV 0.45- $\mu\text{m}$  filter units (Millipore) before injection into rabbits.

**Antiserum Preparation**—Polyclonal rabbit antiserum raised against GS/M H7 trophozoites was described previously (16). Polyclonal antisera specific for the conserved VSP carboxyl terminus were raised in female New Zealand White rabbits by immunization with keyhole limpet hemocyanin conjugates of peptides A or B. Rabbits were injected initially with 1 mg of conjugate in the Ribi adjuvant system and boosted twice at 4-week intervals with 0.5 mg of conjugate; antigen was administered according to the suggestions of the manufacturer. Peptide-specific reactivity of hyperimmune sera was established by enzyme-linked immunosorbent assay using plates coated with the bovine serum albumin-peptide conjugates.

**Electrophoretic and Immunoblot Analysis**—One- and two-dimensional polyacrylamide gel electrophoreses (25) were performed with a Bio-Rad minigel apparatus as recommended by the manufacturer. The ampholyte combination for the isoelectric focusing dimension of the two-dimensional gels was 20% pH 3–10, 80% pH 4.0–6.0 (Bio-Lyte, Bio-Rad), to obtain maximal resolution at the predicted pI of the protein (10). Gels were stained with either Coomassie Brilliant Blue or Bio-Rad Silver Stain Plus according to the manufacturer's instructions. Electrophoretic transfer of proteins to nitrocellulose was at 30 V for 10 h in 20 mM Tris, 150 mM glycine, 20% methanol (26). Filters were blocked with 3% defatted milk, 0.1% Tween 20, PBS for 1 h. VSP H7 was visualized either by reacting with the mouse mAb G10/4, the rabbit polyclonal antisera anti GS/M isolate, or the rabbit polyclonal antisera against the

<sup>2</sup> J. K. Inman and A. Lees, unpublished method.

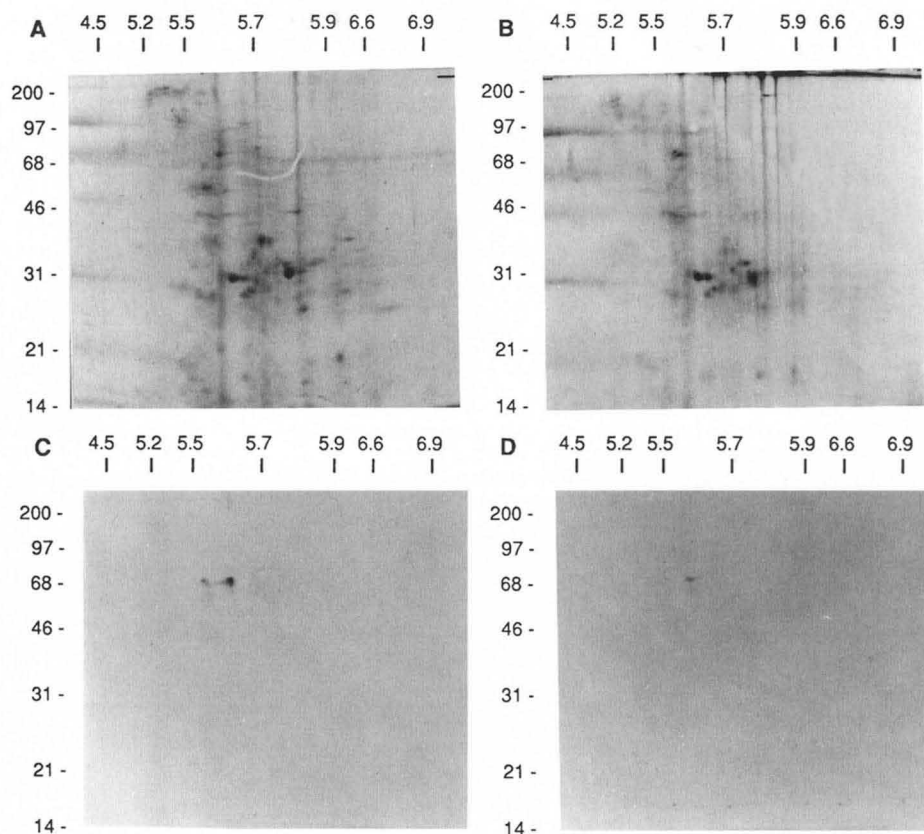


FIG. 2. Two-dimensional SDS-PAGE and immunoblotting analysis of total trophozoite proteins and purified VSP H7. Silver-stained two-dimensional gels of total cell proteins (A), detergent extract (B), and purified VSP H7 (C) obtained as was described under "Experimental Procedures." Immunoblot (D) of the purified VSP H7 using a rabbit anti-serum raised against GS/H7 trophozoites (1:1000 dilution). Top labels indicate isoelectric points and right labels indicate relative mobility of the standards in kDa (Bio-Rad).

COOH-terminal peptides. Polyclonal and mAb antibodies were used at the dilution specified in the figure legend.

**EXAFS and X-ray Microanalysis**—Data were collected at the National Synchrotron Light Source on beamline X-9B using a Si[111] crystal monochromator. The x-ray EXAFS data of the Zn K- $\alpha$  signal from *Giardia* cells were collected using a 13-element energy resolving Germanium detector (27). The x-ray microanalysis data, performed for cells and purified VSP H7, were collected from the center element of the array. The incident x-ray beam energy was set at 10.5 keV, and the energy-dispersive x-ray fluorescence spectra were recorded by a Canberra Ge detector and a multichannel analyzer. The detector was placed at an angle of 90° to the incident x-ray beam so that incoherent scattering from the highly polarized synchrotron beam is minimized. Data were collected at low temperature as for EXAFS. The x-ray microanalysis spectra shown in Figs. 4 and 5 are the observed counts with a correction for the background made by subtracting a spectrum of a pure water sample. The spectrum of a series of zinc acetate samples was also collected in the same geometry and with the same path lengths (1 mm) to create a calibration curve to determine the concentration of zinc in the *Giardia* samples. This allowed us to determine the zinc concentration fairly accurately (0.43 mM), with an error mostly determined by the unknown density of the *Giardia* sample in paste form. The iron concentration could be estimated based on the ratio of zinc/iron counts if the following three corrections were made: 1) differences in zinc/iron cross-sections, 2) higher fluorescence yields for zinc, 3) less reabsorption of zinc fluorescence by the medium (which was assumed to be water in this case). Thus, although the ratio of zinc/iron-integrated counts was 2.5/1 for the *Giardia* pellet, the actual ratio of concentrations is lower due to the above three factors. Briefly, the fluorescence probability for zinc is 0.48, for iron it is 0.34, the zinc and iron cross-sections are 2.33 and 1.409, and the attenuation coefficients for Zn K- $\alpha$  and iron K- $\alpha$  are 7.349 and 18.35 cm<sup>-1</sup> (28), respectively. Thus, the net integral of iron counts substantially underestimates the actual concentration by a factor of 4.6 (this also takes into account losses due to 100 mm of air and the 0.3-mm beryllium window of the Germanium detector). Thus, for the *Giardia* pellet the ratios of counts for zinc/iron of 2.5/1, the elemental ratio is 1/1.85. The methods for collecting zinc EXAFS data have been published previously (29, 30). Data were acquired at 150 K using a helium Displex. For the data shown in Figs. 6 and 7, 16 scans with internal total count rates of 40,000 channel<sup>-1</sup> s<sup>-1</sup> or less were co-added. The Fourier-transformed data were filtered with a window from 1.40 to 2.7 Å<sup>-1</sup> and back-transformed. The fitting range was 4–11.75 Å<sup>-1</sup>.

## RESULTS AND DISCUSSION

The surface location, abundance, and capacity for antigenic variability of VSPs suggest an important role for these proteins in the interaction between the parasite and immune and non-immune components of the host small intestine (3–5, 12–14). To better understand the function of these proteins, we purified VSP H7, expressed by the human *G. lamblia* isolate GS/M, clone H7, by detergent extraction and one-step immunoaffinity chromatography. We constructed an immunoaffinity column by coupling mAb G10/4 (16) to glutaraldehyde-activated Trisacryl<sup>®</sup> (IBF). This hydrophilic support, obtained by the polymerization of *N*-acryloyl-2-amino-2-hydroxymethyl-1,3-propanediol, together with use of 0.1% Thesit in the chromatographic buffers, allowed the purification of VSP H7 at a yield of approximately 13%. Two-dimensional SDS-PAGE and silver staining revealed high degree of purification (Fig. 2C). The purity of the preparation was also confirmed by Western blot analysis using polyclonal antisera against GS/M-H7 trophozoites (Fig. 2D); no other proteins were detected. mAb G10/4 detected the same single species (not shown). Relative to standards, VSP H7 migrated at ~55 kDa with a pI of 5.3 (Fig. 2, C and D). These determinations agree well with the  $M_r$  of 55,344 and a pI of 5.28 calculated for the deduced VSP H7 amino acid sequence, assuming removal of a 14-residue amino-terminal signal peptide predicted by the algorithm of von Heijne (31). Cleavage of this putative signal peptide was verified by the amino-terminal sequence of the purified protein (Fig. 1). In addition, the sequences of two internal proteolytic fragments of the purified VSP were identical to those predicted from the gene (Fig. 1). When compared against a nonredundant data base that included PDB, SwissProt, PIR, and GenPept as well as updates (as of April 3, 1995), peptide 1 (Fig. 1, residues 93 through 110) identified only VSP H7 while peptide 2 (Fig. 1, residues 394 through 406) identified VSP H7 as well as the corresponding regions of other VSPs with identities ranging

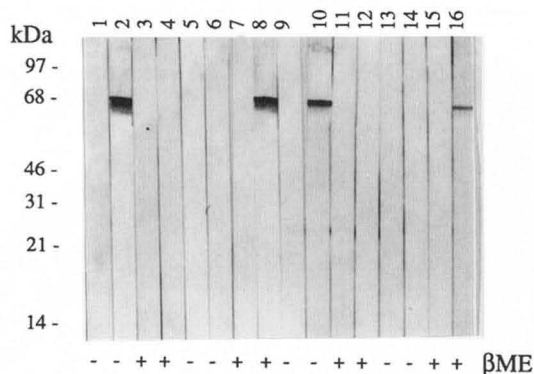


FIG. 3. Comparative immunoblot analysis of total trophozoite proteins and purified VSP H7 using COOH-terminal peptide-specific antisera. Immunodetection by mAb G10/4 (lanes 2, 4, 10, 12), control ascites (lanes 1, 3, 9, 11), preimmune rabbit serum (lanes 5, 7, 13, 15), and immune rabbit anti-COOH-terminal peptide serum (lanes 6, 8, 14, 16), in total trophozoite proteins (lanes 1–8) or in purified VSP H7 (lanes 9–16). Reduction of the sample by  $\beta$ -mercaptoethanol is indicated at the bottom.

from 53 to 70%. Considered together, these data provide compelling evidence that the immunoaffinity purified protein corresponds to VSP H7.

The mobility of VSP H7 in SDS-PAGE and its calculated pI suggest that the protein is monomeric and lacks significant post-translational modification. Consistent with this suggestion, and despite the presence of two potential sites of *N*-glycosylation (Fig. 1, *bold type*), carbohydrate analysis indicated that VSP H7 is not glycosylated (results not shown).

We previously suggested that the absolute conservation of primary structure at the carboxyl termini of VSPs reflects a selection for an important biological function (15). However, no published data indicate that either the COOH-terminal pentapeptide or the putative transmembrane domain are present on membrane-associated VSP. In order to assess the presence of the conserved carboxyl-terminal pentapeptide in VSP H7, and perhaps generate a panreactive VSP antiserum, we raised specific antibodies to synthetic peptides corresponding to the seven carboxyl-terminal VSP residues. Among total trophozoite proteins, hyperimmune antipeptide sera specifically recognized a species of comparable mobility to that detected with mAb G10/4 (Fig. 3, compare lane 8 with lane 2). In contrast to mAb G10/4, which recognizes a VSP H7 epitope sensitive to reduction, the antipeptide sera required reduction of the sample for reactivity (Fig. 3, compare lanes 6 and 8). The identity of this species as VSP H7 was confirmed by analysis of the purified protein (Fig. 3, lanes 10 and 16). These data indicate that the conserved COOH-terminal pentapeptide, which contains two charged residues and is unlikely to be buried in the lipid bilayer, is present on VSP H7. VSPs are not modified by the addition of a glycosylphosphatidylinositol anchor (32) or by prenylation.<sup>3</sup> We infer, therefore, that this protein is anchored in the plasma membrane by the putative transmembrane domain.

Previous reports (13, 14) indicated that VSPs bind zinc, iron, and other similar metal ions *in vitro*. To determine the levels and types of metal ion present in *Giardia* and specifically in VSPs, we performed x-ray microanalyses on both samples and collected EXAFS data on *Giardia* cells.

The energy-dispersive spectra of *Giardia* and VSP samples (Fig. 4 and 5, respectively) show elemental peaks with x-ray energy of 2500 eV and greater exhibited directly. Since these experiments were not performed in vacuum, elements with

energies lower than 6000 eV were attenuated. The major elements in *Giardia* were zinc, iron, and potassium, with small quantities of manganese and nickel. In purified VSP the major elements were zinc and iron. For *Giardia* cell pellets, the observed fluorescent count rate of the Zn K( $\alpha$ ) peak was compared with the signal from defined samples examined in a frozen water matrix. As discussed under "Experimental Procedures," the zinc concentration was determined by comparison with standard samples and the iron concentration was calculated based on known physical constants (28). The measured zinc concentration was 0.43 mM and the calculated iron concentration was 0.80 mM. The levels of these metals in relation to copper were unusually high (33). Also, the similarities in the x-ray microanalysis results with respect to ratios of transition metal ions raises the possibility that our results in *Giardia* are due to the metal content of the VSP.

In order to determine the zinc ion environment in *Giardia*, zinc EXAFS data were separately collected on zinc meso-tetraphenylporphyrin (ZnTPP) and zinc sulfide (ZnS) models to provide amplitude and phase shift information, so as to calibrate the data with respect to interatomic distances and coordination number (30). The data were manipulated to remove the contribution from the absorption edge and these "background subtracted" data are shown in Fig. 6. Data were Fourier-transformed to convert to a radial distribution function, and the *Giardia* Fourier-transformed data are shown in Fig. 7. The Fourier-transformed data show the neighboring atoms of the central metal environment directly. That is, the back-scattering of the atoms in the metal ion vicinity are exhibited. The main peak shows the atoms directly bounded to zinc. However, the Fourier-transformed data only show the relative radial distances of these neighbor atoms. The actual distances of the liganded atoms are at the observed relative radial distance plus a phase shift, which depends on the chemical nature of the back-scattering atom. The first shell peak for *Giardia* is seen in Fig. 7 to be at 2.0 Å. The first shell peak for the ZnTPP, which has four nitrogens coordinating to zinc at an actual average distance of 2.04 Å, was 1.8 Å (not shown). The first shell peak for the zinc sulfide model, which has four sulfur atoms coordinated at 2.35 Å, was observed at 2.0 Å (not shown). Thus, the *Giardia* environment at first glance closely resembles the zinc sulfide model. There was very little contribution beyond the first shell except for a clear peak near the limit of observation (5 Å).

The Fourier-filtered data of the *Giardia* sample were fit to Fourier-filtered model data. Data analysis with fixed coordination numbers was carried out as described previously using the Bell Laboratories EXAFS package on a 386 PC (34). We compared several fits with different sulfur:nitrogen (S:N) coordination numbers held fixed in the fitting procedure. Possible Zn-S and Zn-N distances can be easily resolved; however, nitrogen and oxygen are generally not distinguishable. This fitting can define a family of structures consistent with the EXAFS data. However, without additional information on the zinc site structure, a unique solution cannot be provided. We measured the distances, Debye-Waller factors, and energy shift values of these scatterers by Fourier filtering, back-transforming, and nonlinear least squares fitting of the *Giardia* data and comparing the data with models (29, 30, 34–39). The model data are reduced, transformed, and back-transformed identically to the unknown data, so that artifacts of the manipulations cancel out. Data fitting ranges were 4–11.75 Å<sup>-1</sup> and R-space windows for the Fourier filter were generally in the range of 1.4–2.7 Å for the *Giardia* data and the models. With these windows and this data range, over six degrees of freedom are available, so that a two-atom type fit, with coordination num-

<sup>3</sup> Luján, H. D., Mowatt, M. R., Chen, G. Z., and Nash, T. E. (1995) *Mol. Biochem. Parasitol.*, in press.

FIG. 4. X-ray microanalysis of intact *Giardia* cells, incident x-ray beam at 10.5 keV. The zinc and iron elements produce the major x-ray fluorescence seen. Small amounts of manganese and nickel are observed.

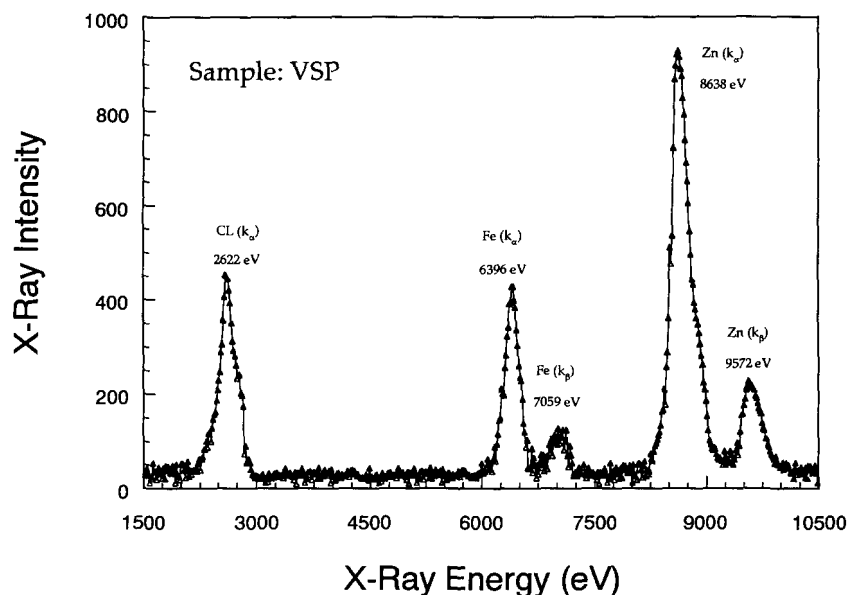
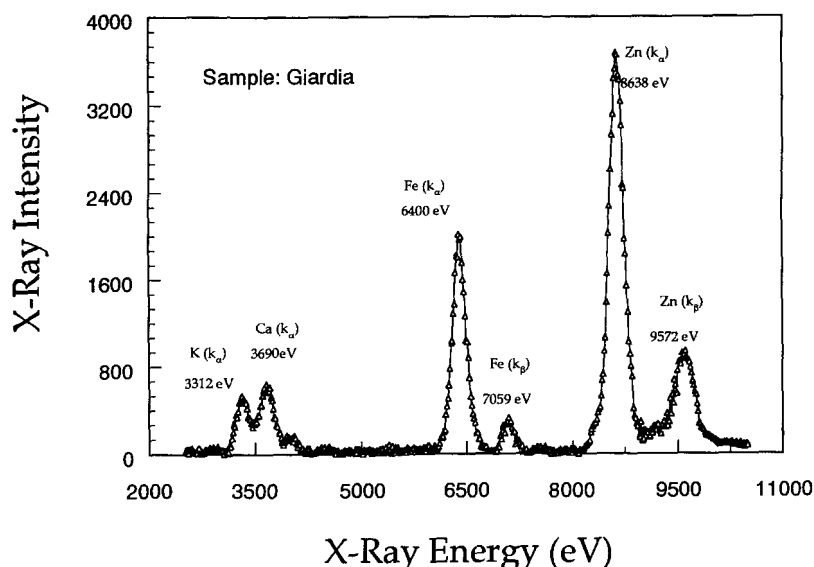


FIG. 5. X-ray microanalysis of purified VSPs, incident x-ray beam at 10.5 keV.

bers fixed, can be supported. However, as can be seen, one atom type fits are sufficient to adequately model the data (Fig. 8). The distance errors are estimated by a number of methods described previously (35, 36). Variations in the individual Zn-S distances were not resolved by this procedure, data of this k-range were unable to resolve contributions that are separated by 0.1 Å or less (35, 36).

Table I shows the results of a series of one- and two-atom fitting procedures. A major uncertainty in this analysis is a distinct knowledge about the heterogeneity of zinc sites for the organism. Zinc enzymes are certainly present in *Giardia*; however, most zinc enzymes demonstrate mostly nitrogen coordination (40). Nevertheless, the data can be modeled adequately by a single type of site with all sulfur ligands. An adequate fit to the data was provided by  $3.8 \pm 0.4$  sulfur ligands at  $2.35 \pm 0.01$  Å distance from zinc. The Fourier-filtered data compared with the fit is shown in Fig. 8. Applying other fixed coordination numbers; including 3–4 sulfurs per 1 nitrogen, resulted in unreasonable Debye-Waller factors or energy shift values for the fit. A reasonable fit was found with a fixed nitrogen contribution of 0.5. However, this reflects the cross-correlation of nitrogen and  $\sigma^2$  in the fit (30, 39, 40). This additional nitrogen contribution does not improve the fit to sufficiently warrant the

additional parameters that are required in the modeling.

Previous investigations of the copper protein stellacyanin and the zinc site of retroviruses illustrated the difficulties in establishing the individual sulfur and nitrogen coordination numbers in cases where both are present, and the total coordination number is four or five (30, 39). This is due to the cross-correlation of parameters in the fit, especially the coordination number and the Debye-Waller factor. The relationship of Debye-Waller factors and amplitudes for the EXAFS equation is such that a more positive Debye-Waller factor tends to reduce the amplitude, while increasing the coordination number has the opposite effect. This is an explanation for how a mixture of site types could be modeled by a single class of sites in the fit, while still having chemically reasonable Debye-Waller factors.

Previous EXAFS studies of the (Cys)<sub>4</sub> zinc finger from the glucocorticoid receptor show minimal back-scattering from the methylene carbons of the cysteine (41). This may be due to disorder in the positions of these carbon atoms. Thus, we do not expect a strong signal from these carbons in a biological back-scattering environment. EXAFS studies of the zinc environment of TF-IIIA (which has two histidine residues), and zinc fingers from retroviruses (which have one histidine in the zinc

FIG. 6. Background subtracted  $k^3$  weighted EXAFS data of intact *Giardia*. This spectrum is the sum of 16 individual scans.

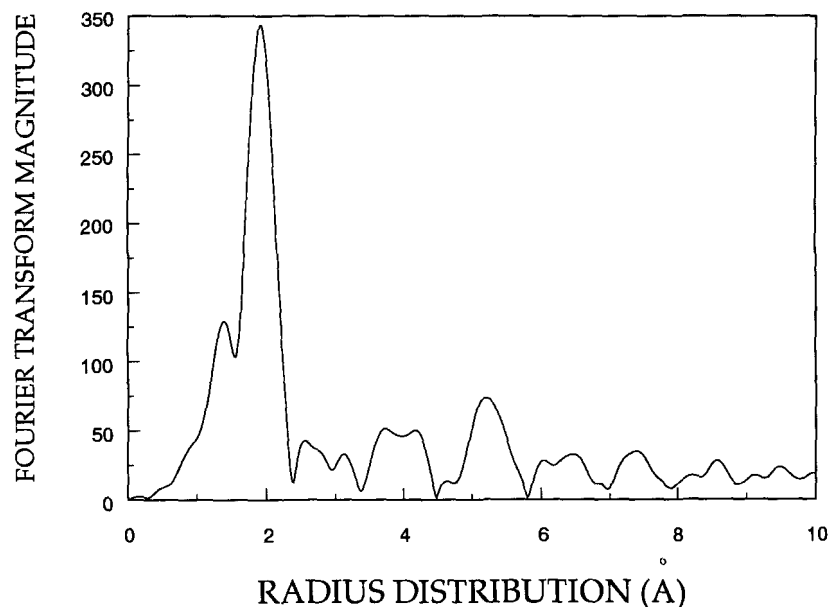
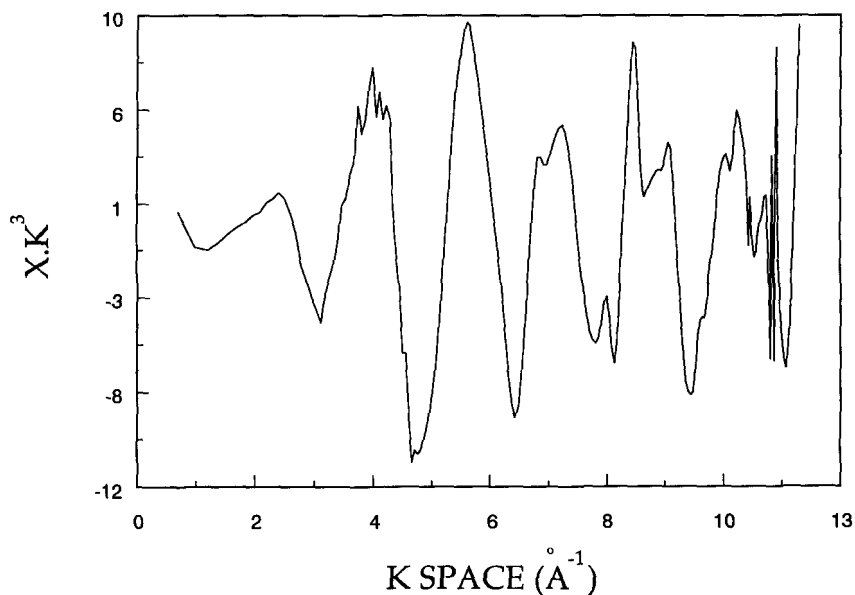


FIG. 7. Fourier transform of Fig. 6. The first shell peak is observed at 2.0 Å, the same position as the Fourier transform of a zinc sulfide model.

TABLE I  
Fitting solutions for *Giardia* EXAFS data

A number of fitting solutions were attempted to model the *Giardia* EXAFS data. Three results are shown to illustrate the overall fitting. A single-atom type was sufficient to model the data. Parameters in bold in the table are chemically unreasonable (30, 39). Attempts to model the site with mixed zinc plus sulfur coordination were unsuccessful except for the use of 0.5 nitrogen atoms in the third solution above. The cross-correlation of coordination number and Debye-Waller factors is such that increased application of the amplitude of a nitrogen model (*i.e.* as the coordination number assigned to nitrogen) results in an unreasonable Debye-Waller factor as that contribution approaches 20% of the ligands (one out of five). It is tacitly assumed that the data could also be adequately fit with zinc-chlorine scatterers, since sulfur and chlorine differ in  $Z$  value by only 1.

Fit type	Model	Nitrogen	$r$	$\Delta\sigma^2$	$\Delta E_0$	$\chi^2$
			Å	Å <sup>2</sup>	eV	
One atom type	ZnS	4	2.35	-0.003	0.15	1.97
Two atom type	ZnS	4	2.35	-0.003	0.91	0.84
	ZnTPP	1	2.00	<b>-0.011</b>	-6.75	
Two atom type	ZnS	4	2.35	-0.003	0.72	0.99
	ZnTPP	0.5	1.98	-0.003	-5.11	

finger site), clearly show higher shell signals due to the pyrrole carbons of the histidine (30, 42). However, the failure to observe such signals in this sample is not conclusive evidence of lack of histidine coordination (29), due to potential disorder of the site. Thus, the zinc environment of *Giardia* is highly un-

usual and is presumptively linked to the metal content of the VSP rather than to cellular enzymes.

Recently, a number of signals characteristic of iron-sulfur clusters have been found in *Giardia*, and ferredoxin was purified from this parasite (43). Since *Giardia* lacks mitochondria

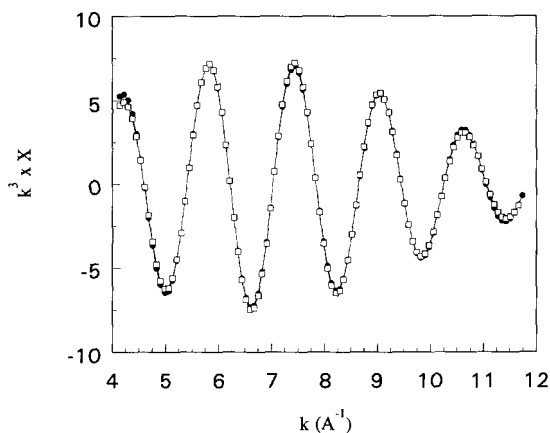


FIG. 8. Fourier-filtered and back-transformed data of Fig. 7 compared with simulated fit data of Table I, the one atom fit with 4 ZnS atoms at 2.35 Å distance. Solid circles represent back-transformed data; squares indicate simulation.

and hydrogenosomes, previous studies suggested the importance of iron-binding proteins in electron transport pathways (1, 2, 44). VSP H7 contains three iron-binding motifs (-CX<sub>2</sub>CX<sub>29</sub>CX<sub>2</sub>C-, Fig. 1), which likely explains the presence of iron in the native protein. This motif as well other iron-binding motifs (45) are present in all the known VSP sequences. Preliminary experiments showed that iron chelators added to *Giardia* culture medium are toxic to the parasite.<sup>4</sup> Nevertheless, the role of VSP in the uptake, reserve, or metabolism of iron by *Giardia* trophozoites remains to be established.

*Giardia* trophozoites thrive in the proteolytic and lipolytic milieu of the upper small intestine. We (5, 13) and others (12, 14) have proposed that the coordination of metals by VSPs could stabilize these proteins, thereby rendering them resistant to proteolytic attack and maintaining the integrity of the cell surface. In this report we provide compelling support for this model, which should serve as a new basis for the rational design of effective therapeutic agents for this important disease. In addition, the ability of VSP to bind zinc suggests an important role for these surface proteins in the pathophysiology of the giardiasis. VSP could bind metals and inhibit important intestinal enzymes such as carboxypeptidases (46). Similarly, VSP metal binding could inhibit zinc or iron absorption contributing to metal deficiency (13, 46).

**Acknowledgments**—We thank Dr. G. Ashwell for carbohydrate analysis, J. T. Conrad for technical assistance, and Dr. R. Fischetti for assistance in the calculation of the iron concentration.

#### REFERENCES

1. Adam, R. D. (1991) *Microbiol. Rev.* **55**, 706–732
2. Thompson, R. C. A., Reynoldson, J. A., and Mendis, A. H. W. (1993) *Adv. Parasitol.* **32**, 71–160
3. Pimenta, P. F. P., da Silva, P. P., and Nash, T. (1991) *Infect. Immun.* **59**, 3989–3996

4. Gillin, F. D., Hagblom, P., Harwood, J., Aley, S. B., Reiner, D. S., McCaffery, M., So, M., and Guiney, D. G. (1990) *Proc. Natl. Acad. Sci. U. S. A.* **87**, 4463–4467
5. Nash, T. E. (1992) *Parasitol. Today* **8**, 229–234
6. Nash, T. E., Banks, S. M., Alling, D. W., and Merritt, J. W., Jr. (1990) *Exp. Parasitol.* **71**, 415–421
7. Nash, T. E., Aggarwal, A., Adam, R. D., Conrad, J. T., and Merritt, J. W., Jr. (1988) *J. Immunol.* **141**, 636–641
8. Nash, T. E., Herrington, D. A., Levine, M. M., Conrad, J. T., and Merritt, J. W., Jr. (1990) *J. Immunol.* **144**, 4362–4369
9. Gottstein, B., Harriman, G. R., Conrad, J. T., and Nash, T. E. (1990) *Parasite Immunol.* **12**, 659–673
10. Nash, T. E., and Mowatt, M. R. (1992) *Mol. Biochem. Parasitol.* **51**, 219–228
11. Aggarwal, A., Merritt, J. W., Jr., and Nash, T. E. (1989) *Mol. Biochem. Parasitol.* **32**, 39–48
12. Aley, S. B., and Gillin, F. D. (1993) *Exp. Parasitol.* **77**, 295–305
13. Nash, T. E., and Mowatt, M. R. (1993) *Proc. Natl. Acad. Sci. U. S. A.* **90**, 5489–5493
14. Zhang, Y.-Y., Aley, S. B., Stanley, S. L., Jr., and Gillin, F. D. (1993) *Infect. Immun.* **61**, 520–524
15. Mowatt, M. R., Aggarwal, A., and Nash, T. E. (1991) *Mol. Biochem. Parasitol.* **49**, 215–228
16. Aggarwal, A., Merritt, J. W., Jr., and Nash, T. E. (1989) *Mol. Biochem. Parasitol.* **32**, 39–48
17. Keister, D. B. (1983) *Trans. R. Soc. Trop. Med. Hyg.* **77**, 487–488
18. Luján, H. D., and Nash, T. E. (1994) *J. Eukaryot. Microbiol.* **41**, 169–175
19. Gabriel, O., and Ashwell, G. (1992) *Glycobiology* Vol. 2, pp. 437–443, IRL Press, Oxford
20. Marck, C. (1988) *Nucleic Acids Res.* **16**, 1829–1836
21. Mantei, N. (1992) *AnalyzeSignalase* (published electronically on the Internet, available via anonymous ftp from ftp.bio.indiana.edu.molbiol)
22. Altschul, S. F., Gish, W., Miller, W., Myers, E. W., and Lipman, D. J. (1990) *J. Mol. Biol.* **215**, 403–410
23. Devereux, J., Haerberli, P., and Smithies, O. (1984) *Nucleic Acids Res.* **12**, 387–395
24. Fujiwara, K., Matsumoto, N., Yagisawa, S., Tanimori, H., Kitagawa, T., Hirota, M., Hiratani, K., Fukushima, K., Tomonaga, A., Hara, K., and Yamamoto, K. (1988) *J. Immunol. Methods* **112**, 77–83
25. Laemmli, U. K. (1970) *Nature* **227**, 680–685
26. Towbin, H., Staehelin, T., and Gordon, J. (1979) *Proc. Natl. Acad. Sci. U. S. A.* **76**, 4350–4354
27. Cramer, S. P., Tench, O., Yocum, M., and George, G. N. (1988) *Nucl. Instrum. Methods* **266B**, 586–591
28. *X-ray Data Booklet, PUB-490 Rev* (1986) (Vaugh, D., ed) Center for X-ray Optics, Lawrence Berkeley Laboratories, Berkeley, CA
29. Summers, M. F., Henderson, L. E., Chance, M. R., Bess, J. W., South, T. L., Blake, P. R., Sagi, I., Perez-Alvarado, G., Sowder, R. C., Hare, D. R., and Arthur, L. O. (1992) *Protein Sci.* **1**, 563–574
30. Chance, M. R., Sagi, I., Wirt, M. D., Frisbie, S. M., Scheuring, E., Chen, E., Bess, J. W., Henderson, L. E., Arthur, L. O., South, T. L., Perez-Alvarado, G., and Summers, M. F. (1992) *Proc. Natl. Acad. Sci. U. S. A.* **89**, 10041–10045
31. von Heijne, G. (1986) *Nucleic Acids Res.* **14**, 4683–4690
32. Das, S., Traynor-Kaplan, A., Reiner, D. S., Meng, T.-C., and Gillin, F. D. (1991) *J. Biol. Chem.* **266**, 21318–21325
33. Thiel, E. C., and Raymond, K. N. (1994) *Bioinorganic Chemistry* (Bertini, I., ed) Vol. I, pp. 1–35, University Science Books, Mill Valley, CA
34. Scheuring, E., Sagi, I., and Chance, M. R. (1994) *Biochemistry* **33**, 6310–6315
35. Lee, P., Citrin, P., Eisenberger, P., and Kincaid, B. (1981) *Rev. Mod. Phys.* **53**, 769–806
36. Lytle, F., Sayers, D., and Stern, E. (1989) *Physica B (Amsterdam)* **158**, 701–722
37. Sagi, I., Wirt, M. D., Chen, E., Frisbie, S., and Chance, M. R. (1990) *J. Am. Chem. Soc.* **112**, 8639–8644
38. Rowlett, R. S., Chance, M. R., Wirt, M. D., Siderlinger, D. E., Royal, J. R., Woodroff, M., Wang, Y.-F. A., Saha, R. P., and Lam, M. G. (1994) *Biochemistry* **36**, 13967–13976
39. Peisach, J., Powers, L., Blumberg, W. E., and Chance, B. (1982) *Biophys. J.* **38**, 277–285
40. Bertini, I. (1994) *Bioinorganic Chemistry* (Bertini, I., ed) Vol. I, pp. 37–106, University Science Books, Mill Valley, CA
41. Freedman, L. P., Luisi, B. F., Korszun, R., Basavappa, R., Sigler, P. B., and Yamamoto, K. R. (1988) *Nature* **334**, 543–546
42. Diakun, G. P., Fairall, L., and Klug, A. (1986) *Nature* **324**, 698–699
43. Ellis, J. E., Williams, R., Cole, D., Cammack, R., and Lloyd, D. (1993) *FEBS Lett.* **325**, 196–200
44. Townson, S. M., Hanson, G. R., Upcroft, J. A., and Upcroft, P. (1994) *Eur. J. Biochem.* **220**, 439–446
45. Bachmayer, H., Piette, L. H., Yayunobu, K. T., and Whiteley, H. R. M. (1967) *Proc. Natl. Acad. Sci. U. S. A.* **57**, 122–125
46. Udomkesmalee, E., Dhanamitta, S., Sirisinha, S., Charoenkiatkul, S., Kramer, T. R., and Smith, J. C., Jr. (1992) *Am. J. Clin. Nutr.* **56**, 50–57

<sup>4</sup> H. D. Luján, unpublished results.